

Short Takeoff Performance using Circulation Control

Tyler Ball*, Scott Turner*, and David D. Marshall†
California Polytechnic State University, San Luis Obispo, CA 93401, USA

Historically, powered lift takeoff analysis has been prohibitively expensive for use in preliminary design. For powered lift, the coupling of aircraft systems invalidates traditional simplistic methods often used in early aircraft sizing. This research creates a tool that will automate the process of takeoff and balanced field length calculations for a circulation control wing aircraft. The process will use high fidelity techniques, such as computational fluid dynamics in order to capture the coupled effects present in circulation control along with Gaussian processes to create a metamodel of that same data to be implemented in a modular takeoff/BFL model. The model was used to examine the performance of a STOL transport and it showed an optimal flap deflection of 64° and diminishing returns on mass flow rates exceeding 12 kg/s. Additional analysis of the STOL transport showed that delaying either the mass flow or the flap deflection until later in the ground roll reduced the balanced field length by up to 8%. In the process of creating the takeoff code, additional consideration was put into the determination of the rotation velocity. It was found that a relationship between lift to weight better defined the rotation velocity with the circulation control model and was found to be within about 10% of traditional techniques.

Nomenclature

b	=	wing span	S	=	Distance for takeoff segment
BFL	=	Balanced Field Length	U _e	=	Local Velocity
c	=	chord	U _∞	=	Free stream Velocity
CC	=	Circulation Control	W	=	Weight
CCW	=	Circulation Control Wing	α	=	angle of attack
C _d C _D	=	2-D and 3-D Drag Coefficient	Subscripts		
C _b C _L	=	2-D and 3-D Lift Coefficient	g	=	ground roll
C _{Lmax}	=	Maximum Lift Coefficient	lo	=	lift off
C _μ	=	blowing coefficient	ob	=	obstacle
OEI	=	One Engine Inoperative	r	=	rotation
q	=	dynamic pressure	to	=	takeoff
Re	=	Reynolds Number			

I. Introduction

Takeoff is frequently primary constraint on an aircraft during the initial design phase, especially in the case of short takeoff and landing designs. These Designs require a huge amount of lift which is often unattainable to even the most sophisticated flap and slat system. Boeing's C-17 utilizes externally blown flaps (EBF) to get its short takeoff while one of Boeing's earlier designs, the YC-14, employed upper surface blowing (USB). Although EBF and USB can generate similar amounts of lift, other details including survivability, maintenance, and cruise performance differ greatly between the two. A third high lift technique which, like USB, utilizes a Coanda effect to generate lift is circulation control. It works by ejecting a thin sheet of air about a rounded trailing edge which in turn causes supercirculation and provides artificial camber without requiring enormous and mechanically complicated flap systems. Although no production aircraft have been built using circulation control, in 1979 the Navy's modified A-6

* Graduate Student, Aerospace Engineering, student member AIAA

† Assistant Professor, Aerospace Engineering, senior member AIAA

successfully demonstrated the system while achieving approach speeds 35% slower and landing rolls 37% shorter¹. Each of the previously mentioned aircraft were specifically designed or modified to takeoff in extremely short distances and their designs revolved heavily around those requirements. In order to properly understand how to predict the takeoff performance of a short takeoff and landing (STOL) aircraft, it is necessary to clearly understand the details and components of a takeoff and balanced field length (BFL).

Takeoff performance can best be analyzed by decomposing the takeoff run into smaller segments. The major segments include the ground roll, the transition phase, and the climb phase. The separation points between these segments are usually determined by critical velocities. These velocities are closely coupled with the lift of the aircraft and are either estimated as a function of the stall speed or can be calculated explicitly if enough information is known about the aircraft. A summary of the different speeds and their locations can be seen in Figure 1 from reference 2.

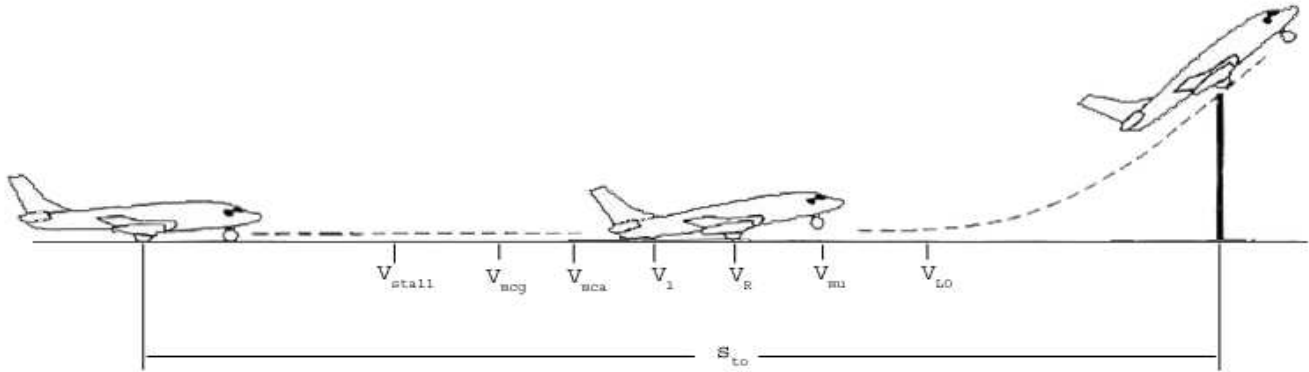


Figure 1: Takeoff Critical Speeds and Components²

All of the critical speeds during the takeoff run have been defined by the FAA³ in order to allow for minimum standards to be achieved by certified aircraft. The regulations therein detail information on most any circumstance including required pilot skill level, braking coefficients for aborted takeoffs, one-engine inoperative (OEI) requirements, and much more. The most critical point in the takeoff run is defined as V_1 by most authors and is called

the decision or critical speed. This speed denotes the maximum velocity at which if an engine failed, the pilot still has time to abort the takeoff and stop safely. This is where the term “Balanced Field Length” originates. The takeoff distance is said to be “balanced” if the braking distance is equal to the takeoff distance for an engine out scenario, as seen in Figure 2 from reference 4. There is no set relationship as to how the decision speed is related to the stall speed. However, the decision speed is bounded on the lower end by the minimum control speed, V_{mc} , which is the minimum speed required for yaw control in the case of engine failure and on the upper end by the rotation speed, V_R . The speed at which rotation occurs is defined as being greater than greater than $1.05V_{mc}$ and less than the liftoff speed⁴. The “minimum unstick speed”, or V_{mu} can be defined as “the airspeed at and above which it can be demonstrated by means of flight tests that the aircraft can safely leave the ground and continue the takeoff.”⁴ This velocity can also be estimated as the speed at which the fuselage tail can strike the ground prior to liftoff. Once the aircraft has reached this point, liftoff then occurs at V_{lo} which is usually around $1.1V_{stall}$. The final critical speed occurs upon clearing the 35 or 50 foot obstacle and is defined as the safety speed V_2 . Most authors define the minimum V_2 to be $1.2V_{stall}$.

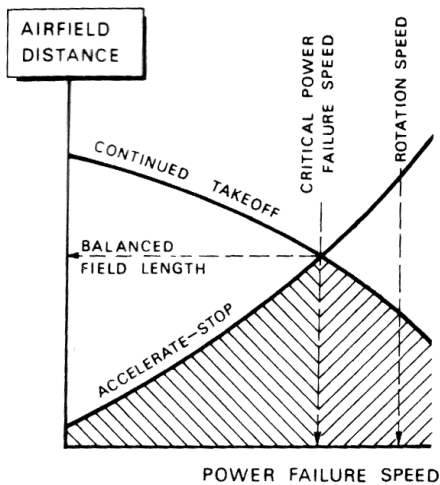


Figure 2: Balanced Field Length³

With all of the details of a takeoff and balanced field length clearly defined, it is necessary to discuss how they are calculated in preliminary aircraft design and the limitations of those calculations with respect to any kind of powered lift.

II. Problems with Balanced Field Length for Powered Lift Aircraft

For preliminary design there is a serious lack in fidelity for balanced field length calculations. The traditional design texts rely on the balanced field length equation from Torenbeek's design book⁴, which is an equation based on the compilation of aircraft flight data. Equation(1) shown below is useful when the aircraft falls within the range of the aircraft used to calibrate the equation; however, it becomes inaccurate when moving into the STOL transport design space.

$$BFL = \frac{0.863}{1 + 2.3 * \Delta\gamma_2} \left\{ \frac{W_{TO} / S}{\rho g C_{L_2}} + h_{to} \right\} \left(\frac{1}{\bar{T} / W_{TO} - \mu'} + 2.7 \right) + \frac{\Delta S_{to}}{\sqrt{\sigma}} \quad (1)$$

There are very few datapoints for which to calibrate the equation and many powered lift methods have complex lift and drag profiles across the length of the takeoff trajectory that are not captured with the simple equation. In short, a more complex method is required for balanced field length calculations on aircraft where that performance number is a driving design factor.

One specific problem is the dependence of the balanced field length on the climb C_L . In the Torenbeek⁴ equation, the C_L for climb is calculated from the $C_{L,max}$, which means essentially the equation is based on a constant lift characteristic number. This presents a significant problem when dealing with powered lift aircraft and particularly CCW aircraft. The blowing coefficient is a function of the freestream Mach number such that at low Mach numbers, the blowing coefficient is high for a constant mass flow and at high Mach numbers the blowing coefficient is low. Since the lift coefficient is strongly based on the blowing coefficient, the lift coefficient becomes strongly coupled with the Mach number, which produces high lift and drag at low Mach numbers and lower values at takeoff speeds. This contrasts with traditional aircraft that have relatively constant lift coefficients over the ground run. Fortunately this does not completely invalidate the equation because at low Mach numbers where these C_L and C_D variation are greatest the dynamic pressures are also low which result in forces of less magnitude. However, the Torenbeek⁴ equation is not equipped to deal with any kind of variation in C_L .

Another substantial problem with the equation is the choice of a $C_{L,max}$ for a powered lift aircraft. As mentioned above, the dependency of the lift coefficient on more than angle of attack complicates the actual lift and drag forces on the aircraft. Since the Torenbeek⁴ equation is a function of only a single C_L its lift model is at the mercy of that number, which for a powered-lift aircraft is not a simple calculation. For a traditional aircraft the maximum lift coefficient is based solely on angle of attack, which provides a buffer when rotating an aircraft for takeoff. For a powered lift aircraft that reference point needs to be made with regards to some Mach and blowing setting, both of which strongly affect the actual maximum C_L . The rotation velocity seems like a logical place to define the Mach number for powered lift aircraft, but in traditional preliminary design the rotation velocity is defined by a percentage of the stall velocity, which is calculated from $C_{L,max}$. Thus, there is no clear guideline on how to calculate a $C_{L,max}$ for a powered lift aircraft.

A way around this problem is to redefine the rotation velocity based on the actual lift produced throughout the takeoff run and the weight of the aircraft. During takeoff there should be some point when the lift reaches some percentage of the weight and rotation can be achieved. If the rotation speed can be defined by this metric it would be independent of the C_L and could be applied to any aircraft rather than only traditional designs. At rotation, the lift over weight will be some percentage, constant k , of the lift over weight at stall, which is 1 as seen in Eq(2).

$$\frac{L_{stall}}{W} = k * \frac{L_r}{W} \quad (2)$$

Now, if some common assumptions are used that relate the max lift coefficient to the rotation lift coefficient and the stall velocity to the lift velocity, one can reduce Eq(2) using the following logic. Simplifying Eq(2) yields:

$$L_{stall} = k * L_r$$

$$V_{stall}^2 * C_{L_{max}} = V_r^2 * C_{L_r} * k$$

Below are the equations for the assumptions:

$$V_r = C * V_{stall} \approx 1.05 V_{stall} \quad \frac{C_{L_r}}{C_{L_{max}}} = 0.9$$

Substituting back into Eq(2):

$$\begin{aligned} \frac{V_{stall}^2}{0.9} &= (1.05 V_{stall})^2 * k \rightarrow k = 1.223 \\ 1 &= \frac{1.223 * L_r}{W} \\ \frac{L_r}{W} &= 0.817 \end{aligned} \quad (3)$$

This yields a criterion for when rotation occurs that is not dependent on the actual $C_{L_{max}}$ of the aircraft only the ratio of $C_{L_{rotation}}$ and $C_{L_{max}}$. This follows the same basic format as the other preliminary design guidelines stating that the rotation velocity is a percentage of the stall velocity. This makes it easy to define a rotation speed in a number of different cases using the same flavor of regulations.

The downside for this is the need to have C_L data at each velocity along a ground trajectory in order to figure out where the lift to weight ratio reaches 0.817. However, this is not particularly constraining because it works with a constant C_L model as well as more complicated aerodynamics models. All that is needed is to run a series of test cases and then find the velocity that matches the ratio. Optimization processes could be used if desired but are by no means required. This also works well with an integration of the equation of motions into a trajectory model since all of the required data would be available after the integration.

III. Circulation Control

Since circulation control (CC) was the high lift device used in this study, it is important to overview some of the important features. The idea of using pneumatic devices to augment airfoils has been around since the 1930s⁵. Most of these early designs consisted of either jet flaps or blown flaps which utilized a sheet of air ejected on a flap or at a given angle. The term “circulation control” came by extending the performance of those previous designs by ejecting the flow over a rounded trailing edge as can be seen in Figure 3 obtained from reference 5. The Coanda effect holds the sheet of ejected air to the rounded surfaces and that sheet in turn entrains the external flow around it and directs it downward. The downward deflection can be thought of as a pneumatic flap which effectively increases the camber and lift of the airfoil or wing. Some of the early benefits of CC included the ability to achieve high lift with little flaps or even a fixed trailing edge and the ability to increase lift without a change in angle of attack.

Both of these characteristics prove to be desirable in the design of a STOL transport for obvious reasons.

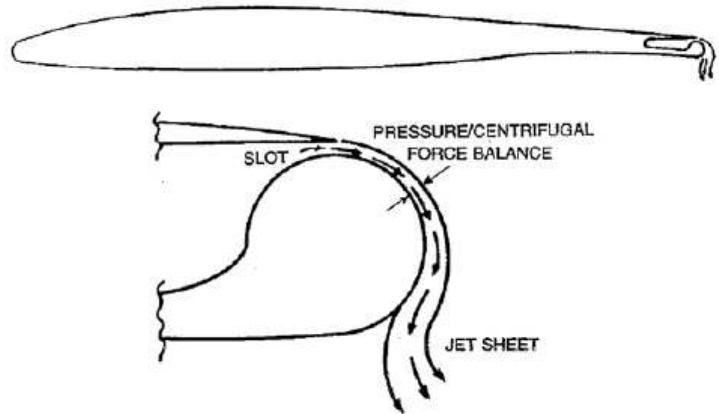


Figure 3: Circulation Control Aerodynamics⁵

A great deal of effort has gone into the design of the trailing edge of CC airfoils. Although it is well established that a rounded trailing edge performs well, it is not well known how large of a radius or even if it should be circular. In addition to the difficulty of deciding the shape of the trailing edge, determining how to best create that shape is another

problem. Some examples of how this has been done can be seen in Figure 4 from reference 6.

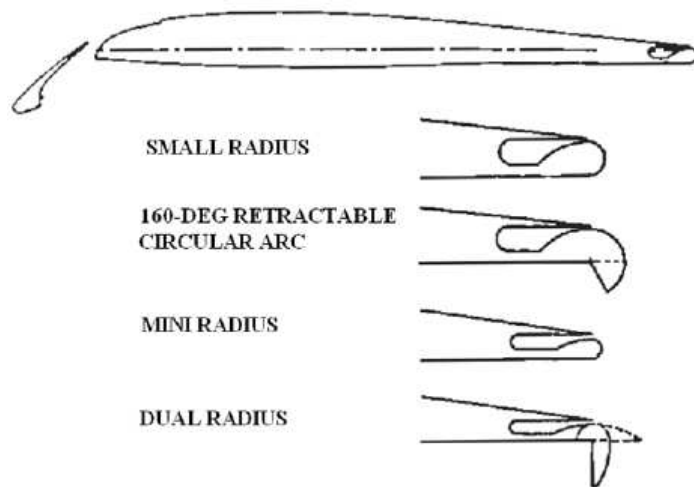


Figure 4: Different Trailing Edge Devices⁶

the flow would be tangentially ejected. After passing over the first radius, the flow then travels past the larger radius which is that of the flap upper surface. This dual radius combination provides a large Coanda surface to facilitate the CC and allows for a sharp trailing edge for cruise flight. For these reasons, the dual radius trailing edge was used for this study.

The basic CC wing geometry for this study was based the Model 114 ESTOL vehicle concept created by the California Polytechnic State University, San Luis Obispo in conjunction with NASA Ames ESTOL sector as an ESTOL study reference vehicle during the summer of 2004⁷, the final configuration which can be



Figure 5: Model 114 ESTOL Vehicle⁶



Figure 6: Circulation Control Wing

seen in Figure 5. The airfoil for the CC wing was based off of the previously mentioned dual radius flap with the basic airfoil based on the NASA SC(2)-0414. A dual radius flap located at roughly 0.9c was added to that airfoil and given a slot height to chord ratio of 0.0016 which is below the 0.002 upper limit where the jet flow then becomes inefficient⁸. Due to symmetry, only half of the wing was required for the CFD model. The half wing, as seen in Figure 6 had a reference area of 36.153 m² with 9.63° of leading edge sweep and a dual radius flap which extended 80% of the span with an area of 0.04459 m². A detail of the dual radius flap can be seen in Figure 7.

One of the difficulties of CC lies in the source of the

air for the ejection slot. An obvious source would be the jet engines already installed on an aircraft. However, the major disadvantage of coupling your high lift device with the propulsion system means that to lose one most likely means to lose both. A solution to this problem would be to cross-duct multiple engines so as to provide redundancy and allow for the loss of an engine without the loss of takeoff or landing capability. A solution which completely decouples the two systems is to embed gas generators in the wings and dedicate them to running the CC system. Although each of those configurations deserves a great deal of thought when analyzing the performance of a CC aircraft, the focus of this study was on the last case with a completely decoupled high lift and propulsion systems.

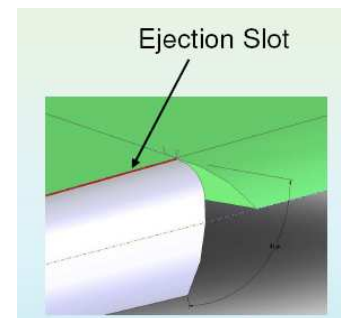


Figure 7: Detail of Dual Radius Flap

IV. CFD: Mesh and Solution Techniques

One of the major drawbacks for the current simplified methods for calculating takeoff distance is their lack of knowledge of how the lift and drag of an airplane vary throughout the takeoff run. Although the simplified models provide adequate results for traditional aircraft, the results for STOL aircraft are largely inadequate. This inadequacy is due to the fact that there are no analytical methods to accurately calculate the lift and drag of an aircraft using powered lift such as circulation control. A previous solution to this problem by Percey and Margason⁹ used available wind tunnel test data and developed a quadratic curve fit relationship between C_{Lmax} and the blowing coefficient for USB. This technique of creating quadratic curve fits to wind-tunnel data was repeated several times throughout their paper in order to establish relationships of how lift, drag, and thrust vary during takeoff. A similar approach was used in this study, the aerodynamics of which will be discussed presently and the metamodeling to be discussed in section VII. CFD was performed on the previously described CC wing over a variety of Mach numbers, angles of attack, flap deflections, and mass flow rates. However, before the full CFD study could be performed, it was necessary to determine which turbulence model would best predict the performance of CC.

Since circulation control involves complex flow as a result of the ejection slot and its interaction with the freestream flow, some turbulence models capture the flow behavior better than others. It was important to make sure the turbulence model behaved well at slow speeds in order for a takeoff run to be properly examined and also to correctly resolve the shear layer at the jet slot. The 2004 CC Workshop co-hosted by NASA and ONR invited its participants to take part in a two-dimensional CFD analysis of a CC airfoil designated NCCR 1510-7067N in order to establish which models and grid types could match experimental results¹⁰. Two models which tended to produce good results were the *Spalart-Allmaras* and $k-\omega$ turbulence models. *Fluent*, which is a commercially available CFD package, provides several different turbulence models from which to choose including *Spalart-Allmaras* and $K-\omega$. In order to establish which of the two turbulence models and what type of grid were to be used, a study was performed in which the results were compared to experimental results obtained by Robert Englar which were reproduced in reference 11. In order to accomplish this, multiple two-dimensional grids were created around the dual radius circulation control airfoil which were then solved under the same conditions as those found in reference 11. These two grids had maximum y^+ values of about 50 and 500 and are thus called the fine and coarse grids. The fine grid was solved using both turbulence models while the coarse grid only with *Spalart-Allmaras*. The lift as a function of blowing coefficient for the different grids and turbulence models can be seen in Figure 8. The coarseness of the grid and the type of turbulence model clearly has a significant impact on the results. The solution that most agrees with the experimental data utilized the coarse grid with the *Spalart-Allmaras* turbulence model. A possible reason for the significant difference between the *Spalart-Allmaras* results could be due to too much refinement in the fine grid. Since it had a maximum y^+ of 50, than a significant portion of the airfoil had lower values which could have put those boundary layer cells within the laminar sublayer which in turn could have introduced some error. At any rate, the *Spalart-Allmaras* model proved to be the better of the two as long as the y^+ was not too small.

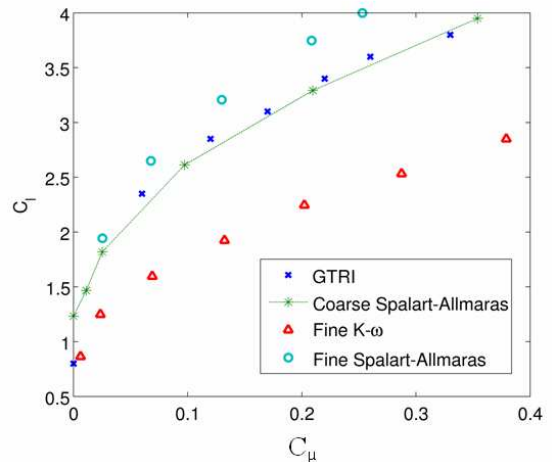


Figure 8: Solver and Grid Comparison

With the turbulence model decided upon, the next obstacle was to obtain 3-D results over the entire 4-dimensional design space which was mentioned previously. The first decision which had to be made was how to cover the design space with data points that would sufficiently capture the relationships between the input variables without requiring an enormous number of cases. These data points would then be metamodeled using Gaussian processes in order to predict the behavior within and even slightly beyond the design space. The details of the metamodeling will be discussed in a later section. It was decided that the best way to capture the entire design space was to perform a full Monte Carlo for each of the 4 input variables. Among other reasons which are discussed in the metamodeling section, randomness provided by the Monte Carlo approach allowed for the resulting data to be orthogonal and also for the design space to be well defined without having to finish any pre-determined number of cases. The 4-D design space was randomized over the following ranges: Mach number from 0.06 to 0.2, angle of attack from -2° to 8° , mass flow rate from 0-20 kg/s, and the dual radius flap deflection from 0- 90° . Each of those ranges well defined the possible

performance during a typical STOL takeoff with the exception of Mach number with the lower limit of 0.06 due to the inability to reach consistently converged solutions at slower speeds. The only other problem with the random points came from the flap deflection. Because of the complexity of the 3-D wing, it was difficult to alter flap deflection within *Gambit*, which is the gridding software companion to *Fluent*. As a result, a new grid was required for each flap deflection. In order to limit time gridding but also clearly define the design space, the random flap deflections were rounded to the nearest 3°. This was decided to be a reasonable simplification because flap deflection was not believed to have sudden jumps or discontinuities in its functionality and would therefore be well defined with 3° intervals. With all of the input variables chosen, the next step involved creating the required 30 grids.

Since very little difference existed in the wing geometry for 3° flap increments, it was the goal to institute an automated method to generate the grids. Although *Gambit* allows the use of pre-written script files to generate grids, the process was never able to be fully automated. The major difficulty came in *Gambit's* inability to keep consistent with reference points given different imported geometries. As a result, the process was only semi-automated. The reference points on each geometry had to be defined by hand for each grid which then allowed for the remaining edge, surface, and volume grids to be completed automatically. The final grids were unstructured with about 1.2 million tetrahedral cells defining the wing surface and flow volume and an example of one of them can be seen in Figure 9. Unlike in two dimensions, three dimensions pose a serious problem for computational time. With the number of cells in the millions in 3-D compared to the thousands in 2-D, the convergence time increases from several minutes to several hours. In order to decrease computational time, several different solution techniques were investigated.

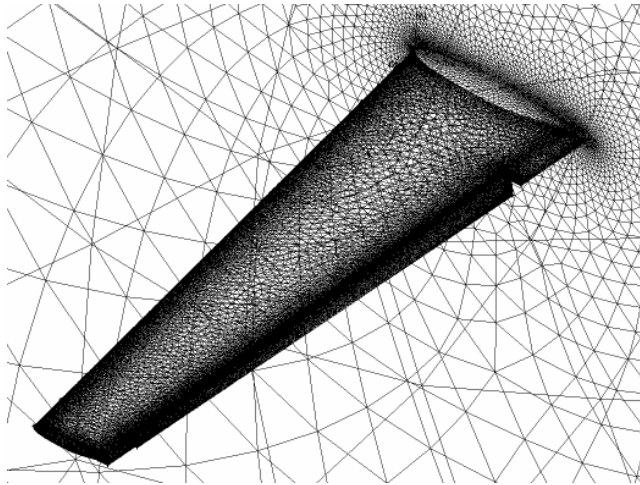


Figure 9: 3-D Unstructured Tetrahedral Grid

A number of different techniques were used to decrease convergence time for the 3-D grids. The goal was to keep the number of cells for each grid to a minimum in order to capture the major flow characteristics and then utilize *Fluent's* grid adaption capabilities to resolve the shear and boundary layers. *Fluent* allows for many different types of grid adaption in order to resolve local flow effects in unstructured grids by dividing the cells in the desired location until the desired resolution is obtained. By adapting the grid with respect to y^+ after it had converged on a coarse grid, *Fluent* was able to lower the y^+ significantly and re-converge with a minimal number of additional iterations. An example of the adaption on the wing surface at the dual radius flap can be seen in Figure 10. It was found that a series of 5 adaptations could reduce the y^+ to a value of 570 which allowed for the effects of the boundary layer to be included in the flowfield. Although the results of the adapted grid looked promising, there was still an issue with computation time. The grids quickly increased in size to over 3 million cells after a couple adaptations which drastically increased convergence time.

The next technique to decrease convergence time which was investigated was the use of multi-gridding. Multi-gridding is a process of using successively coarser grids in order to eliminate low frequency error from the system. This ability is built into *Fluent* and, when enabled, allows the user to generate a specified number of coarser grids and control over many other properties related to the elimination of error from the system. Although sweeping through a series of grids proved to take additional time for each iteration, it was found that the number of iterations required to reach convergence was an order of magnitude lower when multi-gridding was used when compared to a single grid. One of the drawbacks known to exist with multi-gridding is the loss of non-linear flow effects due to the interpolation between grids. To determine whether the

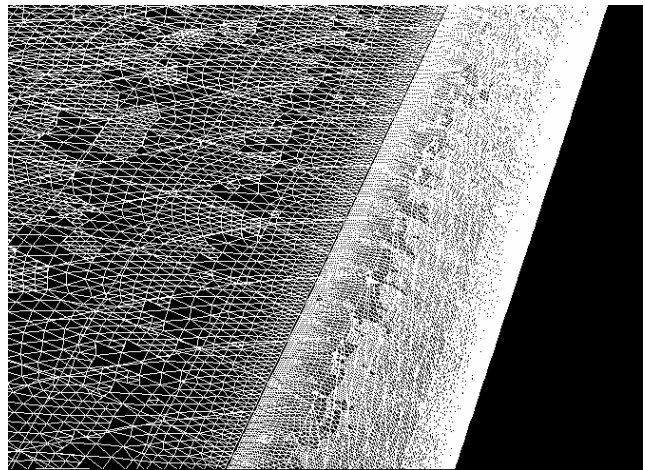


Figure 10: y^+ adaption on the Wing Surface

results for circulation control wing were being altered by the multi-gridding, a case was solved with and without the use of multi-gridding and the resulting C_L was found to be only 1.6% different. Finally, the proper time to implement multi-gridding in order to minimize convergence time was investigated. It was thought that a solution might be obtained quicker if a laminar case was first converged and then the turbulence model was to be turned on. However, this was found not to be the case. The minimum convergence time was found to occur with multi-gridding and the *Spalart-Allmaras* turbulence model enabled throughout the case. It was found that before adaption, convergence occurred in less than 4 hours with 500 iterations. Once adaption was enabled, the time to iterate significantly began to increase which resulted in an additional 8.65 hours to iterate an addition 150 times to reach convergence. A summary of the solver techniques and their performance can be seen in Table 1 for a case with 90° flap deflection, Mach number of 0.0836, angle of attack of 0°, and a jet slot mass flow of 10 kg/s. The pathlines of the flow exiting the ejection slot for the *Spalart-Allmaras* case with multi-gridding and 3 adaptations can be seen in Figure 11.

Table 1: Solver Performance Comparison

Method	# Iterations to Convergence	Run Time (hrs)	Adaption(#)	Y+	CL	CD	CM
Spalart-Allmaras with multi-grid at 2500	3000	15.88	no	8202	2.6234	0.4732	2.0722
Spalart-Allmaras with full multi-grid	650	12.4	yes(3)	638	2.5830	0.4901	2.0450
Spalart-Allmaras with full multi-grid	500	3.75	no	8202	2.5980	0.4700	2.0534
Laminar to Spalart-Allmaras	2000	4	no	9000	2.5550	0.4472	2.0187

The process of setting up a case in *Fluent* involves several steps which can take a long time when many cases are run on several computers. In order to speed up the process, scripts were written that would automatically set up the boundary conditions, turbulence model, multigridding, and the grid adaptations. The script also automatically saved the case at different intervals with a unique name given to each case which included each of the 4 inputs allowing for good organization of the large case files facilitating the importing of the data into a large database. These script files eventually allowed for case files to be set up and run on remote computers in a matter of seconds with minimal input requirements from the user.

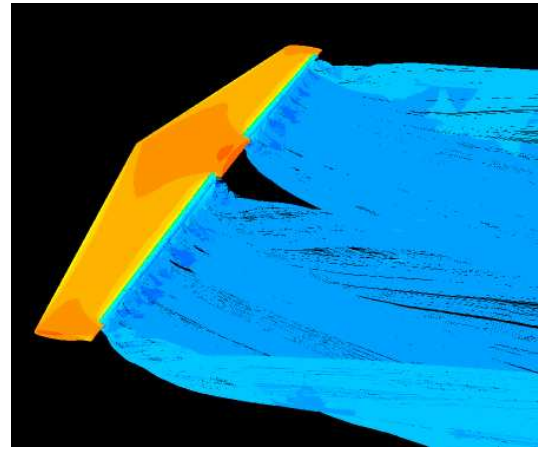


Figure 11: Pathlines from Jet Slot using Multigridding and 3 Adaptions

V. CFD Results

In the end, 40 random cases were solved in order to completely define the 4-D design space. An example of typical results along with some atypical results will briefly be discussed. A typical case occurred at a Mach number of 0.15, an angle of attack of 4°, a mass flow rate of 9.4 kg/s, and a dual radius flap deflection of 66°. Streamlines colored by Mach number at a slice in mid span can be seen in Figure 12. The basic principles and performance of CC can clearly be seen in this figure. The high speed mass flow can clearly be seen ejected over the dual radius flap and continue down into the flowfield. Although the flap is only at 66°, the curvature of the two radii clearly deflect the flow at what appears to be nearly 90°. As a result of this, the forward stagnation point can clearly be seen shifted significantly down the lower surface of wing while the rear stagnation point lies at the tip of the flap. The curvature of the pathlines in the immediate flowfield indicate a significant increase in camber and therefore a reasonably high lift coefficient.

Although Figure 12 illustrates ideal CC characteristics, not all cases in the design space did. Some interesting flow phenomenon began to occur at high angles of attack and high mass flow rates. An example of this can be seen in

Figure 13 with the case defined as follows: Mach number of 0.15, angle of attack of 7.9, mass flow rate of 0.8 kg/s (equivalent to about 20 kg/s for the 3-D wing), and a flap deflection of 88°. Figure 13 is a 2-D case, which more clearly shows the behavior of the 3D results for the same conditions. This case illustrates the near maximum of three of the input parameters: angle of attack, mass flow rate, and flap deflection. The result of this extreme case can be seen by examining the location of the forward stagnation point. The freestream flow is being forced to turn all the way around the leading edge of the wing and then attempt to turn well over 90° at the flap. With the exception of the extremely high speed flow coming out of the slot, almost none of the flow gets entrained completely around the flap. As a result, the peculiar recirculation region appears directly aft of the flap. This loss of entrainment ended up significantly reducing the lift generated by the CC. On a slightly more positive note, the net drag ended up decreasing at the high flap deflections. This was assumed to be a result of the decreased induced drag which decreased more than the added parasite drag from the recirculation region increased. These results led to the idea that there was an ideal flap deflection in order to produce the maximum amount of lift and that it was less than the maximum deflection. More discussion about ideal flap deflections and mass flow rates will be given in the section regarding the performance of STOL aircraft.

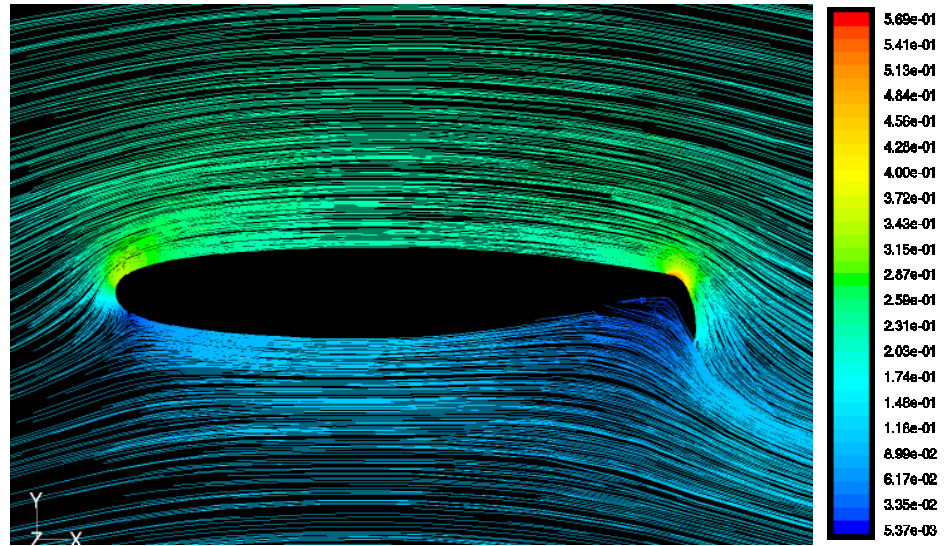


Figure 12: Streamlines Colored by Mach number for a Typical Case

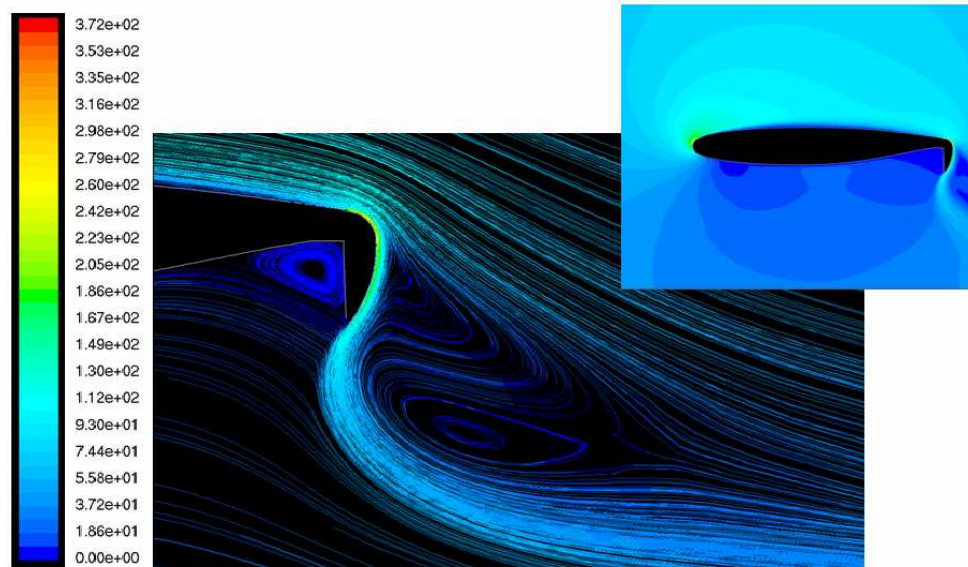


Figure 13: 2-D Streamlines and Contours Colored by Velocity magnitude (m/s) Illustrating Recirculation Region

VI. Database Layout

The database used for this research was a MySQL database with access provided through a text based user interface written in Bash script and Perl. Once an experimenter completed a computer simulation, they ran the script, which finds and stores metamodel parameters in the database. The interface extracted all the data needed from the *Fluent* files' input that into the database and created appropriate linking information. *Fluent* input parameters and solution data (such as C_L , C_D , C_M and jet slot velocity) were all stored and updated in the database. Each experimental case input was tracked by a unique experiment id, which links the data to experiment parameters. The nature of the MySQL database prevents duplicate storage of the same data to insure that only the most relevant data is available for export. To create a metamodel, the data from the database is exported using scripts to a file format that can be read with a custom Matlab Gaussian process modeling tool. To use a different model only the output script need be modified.

An advantage of the MySQL database and script combination is that it is robust and acts as a data hub for any remote Linux or Unix machine. This provides experimenters in different locations the ability to upload data to the database and have it metamodeled remotely. The results of this metamodeling can then be uploaded to the database and any user can access that data. This is particularly beneficial in the case of CFD because large computational cases can be run on computers at different locations and the data can be integrated seamlessly. If the Linux system were overly restrictive to users, it is possible to port the scripts over to other operating systems or to create a web based GUI with additional work.

VII. Meta Modeling

While modeling techniques attempt to predict the behavior of a system, metamodels attempt to predict the behavior of a model. This is useful for models that are expensive to obtain data points, such as CFD experiments, because relatively few points can be used to build a metamodel of the entire design region. It is impractical to calculate design points for the entire design space for CFD situations because takeoff calculations are based on a number of changing parameters, and changing any one parameter requires a new solution that will take at least three hours for the CCW case addressed. This affect was compounded when running an iterative BFL code, which was the final goal of the research. Thus the goal was to build a metamodel that captured all the important flow phenomena and was also quick to evaluate across the entire takeoff range.

The first component was to determine an experimental design for the collection of CCW CFD data points from which to build a model. A variety of model types were investigated including, full factorial, partial factorial, latin hypercube, and full random. The factorial designs were eliminated because statistical analysis is not valid for an incomplete dataset, which limits the usefulness of the design and are typically reserved for experimental datasets with noise error¹². Classic DOE methods do not apply to computer experiments because for a given set of inputs the outputs will always be the same, effectively eliminating the random error. The main source of error for such experiments comes from the bias error of the system, that is, the way in which the metamodel differs from the functional behavior of the model. The latin hypercube and full random cases were examined and the latin hypercube added no additional benefits while adding complexity since a full random case was possible. Therefore, the final scheme was a full random for all of the design variables with the flap deflection discretized into 3 degree increments to cut down on gridding times.

The response data was lift, drag and moment coefficients, which were taken from the *Fluent* runs. The factors that were varied per run were the Mach number, angle of attack, mass flow rate and flap deflection. The Mach number was essential because it was required for use in the balanced field length integration. The angle of attack was needed to model different phases of flight. The mass flow rate was chosen as the common input variable for two reasons. First, the mass flow rate has a large effect on the lift generated by the CCW system. Secondly, the mass flow rate term, which represents the exhaust gas velocity, can be used to model engine out situations. For simplicity, the mass flow rate was set as a constant for the length of a ground run. This was reasonable because the exit velocity and density of the flow exiting the back of the circulation control flap changes only slightly over the course of the takeoff as long as all engines are functioning. Also, the design assumed imbedded gas generators to decouple the thrust producing engines from the mass flow producing engines. Ideally BFL calculations would be conducted on a variety of different engine failure criterion including mass producing engine failure, which could be modeled since the mass flow was included as a factor in the model. Lastly, flap deflection was included because it is another critical component when using CCW to obtain a super-circulation effect.

These factors and responses were modeled using two different metamodeling methods, response surfaces and Gaussian processes. The response surface analysis was done with Matlab's response surface tool and fit a full quadratic model that included quadratic terms in all the factors along with interaction terms for all possible combinations of factors. The result is seen in Figure 14.

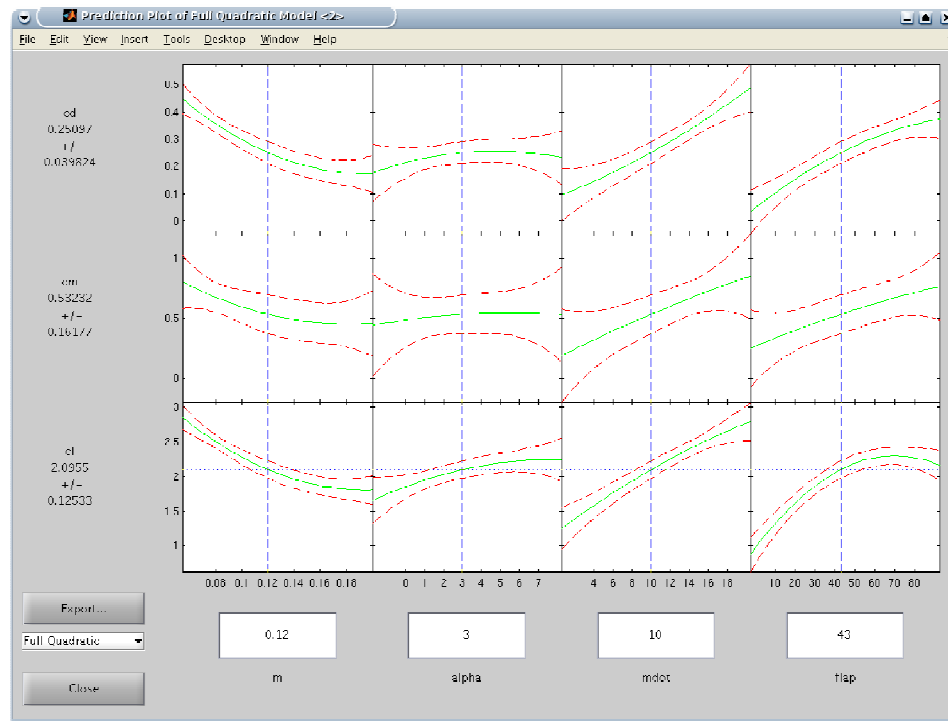


Figure 14: Response Surface Model

The problem with the response surface model is that the analysis for response surfaces is based on a standard statistical model that assumes noise error, normalized residuals, uniform variance, etc., all of which are not valid for metamodeling computer data¹³. While not entirely valid, the response surface did provide a convenient check on general trends in the flow behavior, especially since a tool was already available.

Gaussian process metamodels can be made to deal with noiseless data and the parameters used to define them can be optimized to fit the data. These capabilities were highly desirable for the CFD analysis of CCW aircraft. The Gaussian process models were based off of code written by Carl Rasmussen¹⁴ where the hyper-parameters were chosen based on minimization of the log likelihood. This process is computationally expensive, relative to response surfaces, as the hyper-parameters are optimized by a gradient-based optimizer for the dataset and have to be re-optimized if new data is added and the optimal model is still desired. However, compared to the computational cost for one CFD run, computational time is insignificant. Also, once a model is built and no more data points need to be added, an optimization step is no longer needed further speeding computation times.

An additional benefit of Gaussian process metamodels is that they can better capture complex fluid behavior that a response surface would average out across the entire design space¹⁵. Figure 15 shows one such study where a complex function including exponential, sinusoidal and step function behavior was modeled. It is important to note that to really resolve the step a large number of points were needed which corresponds to a lot of data. This may be impractical depending on the time it takes to get data points but does display the ability to capture such flow features.

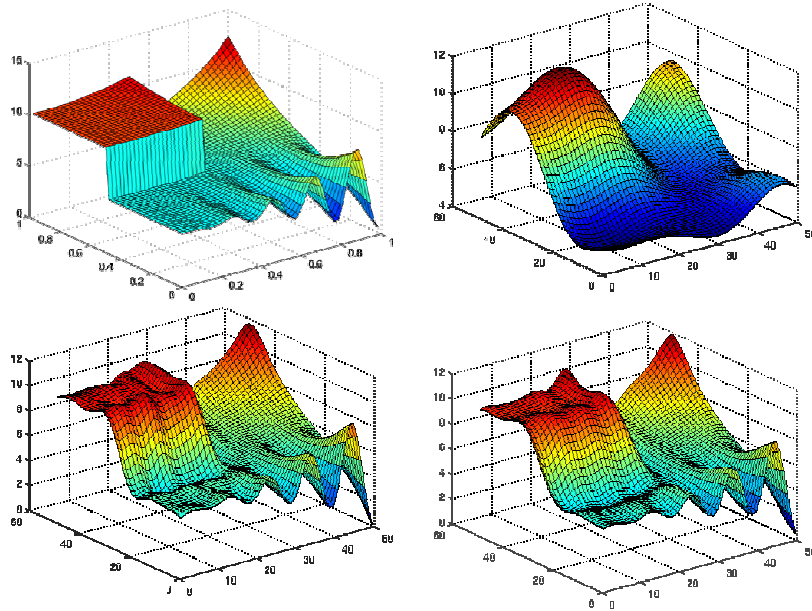


Figure 15: Complex Behavior modeled by Gaussian Process. Clockwise from top left: actual function, Gaussian process model of that function given 100, 500, and 1000 training points

Once the hyper-parameters are optimized they are then used along with the training data points to build the model. The number and effect of hyper-parameters are dependent on the covariance function chosen for the model. Covariance functions are analogous to basis functions in that they define the general shape and behavior of the Gaussian process model, but are still highly flexible. The hyperparameters are coefficients within the covariance functions that define the characteristic length scale of the function. This determines approximately how far the function can go before it has a large change in magnitude. Large length scales correspond to global models where many points affect the overall shape of the model, such as a response surface. Small length scales correspond to models that are affected by only neighboring points, such as splines. This idea is shown in the figure below reproduced from Gaussian Processes for Machine Learning¹⁴, Figure 16.

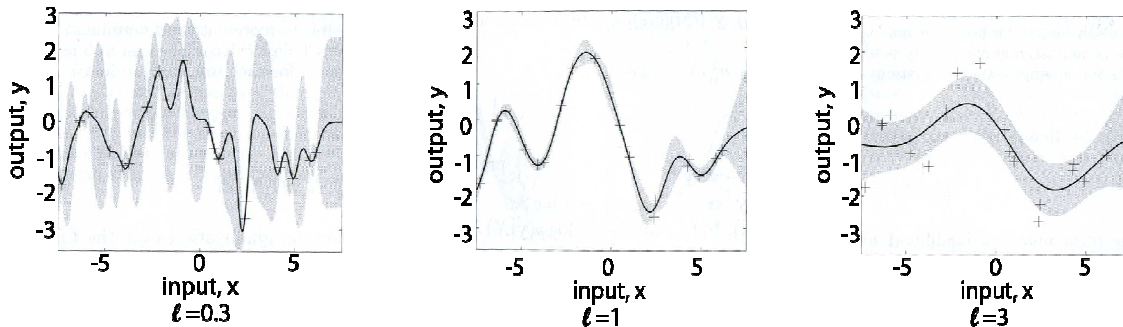


Figure 16: Illustration of the use of Length Scale in Gaussian Processes¹⁰

By optimizing the hyperparameters based on the log likelihood, the model that best fits the points can be created. The covariance function used for the initial work was a squared exponential covariance function, which was chosen to model the smooth behavior expected for subsonic takeoff aerodynamics.

The purpose of creating the model was so that the equations of motion could be numerically integrated over the course of a take-off run and the balanced field length could be calculated for a 3D CCW. Balanced field length calculations are computationally expensive by nature, since balanced field length is defined as the distance traveled to clear an obstacle at the end of the runway or come to a complete stop in the same distance given an engine failure on takeoff. With the engine failure point unknown, the equations of motion must be solved iteratively to establish when an engine out condition yields equivalent braking and takeoff distances. To allow for visual exploration of the design space, a graphical tool was created that allowed for visualization of the multidimensional Gaussian process the same way one could explore a response surface with the Matlab response surface tool, Figure 17.

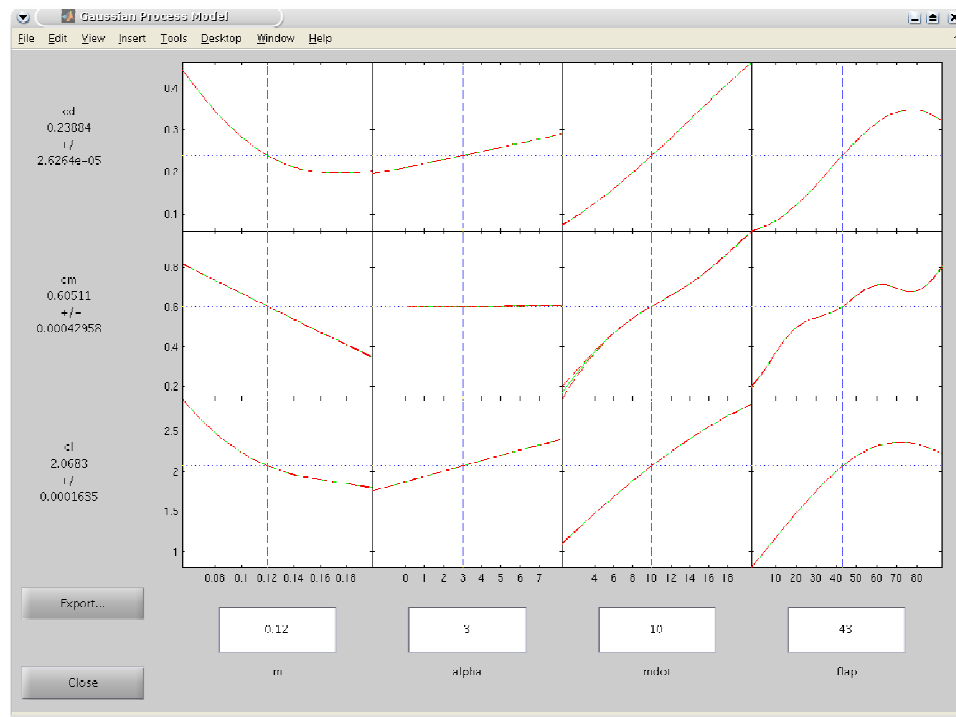


Figure 17: Gaussian Process Graphical Interface

The ability to see individual variable effects was another beneficial advantage of modeling the multivariate data. For example, the Gaussian process was able to capture the loss of lift due to the loss of super circulation at high flap deflections, which could have been missed had a multivariable plot not been used. The loss of lift was noticed in the Gaussian process plot first and then further investigated using *Fluent*, Figure 18 and Figure 13. The velocity vectors show a distinct separation region behind the flap of the wing that interferes with the supercirculation effect decreasing the overall pressure on the bottom of the wing. From Englar¹⁶, dual radius CCW applications are expected to get their best performance at 90 degree flap deflections with leading edge and trailing edge blowing. Thus the results do not match the similar results from Englar¹⁶ and without the metamodel could have been missed simply due to the difficulty of visualizing results in multiple dimensions. The metamodel allowed for a focused look at a particular region of the flow in a large dataset.

The final metamodel consideration addressed was how the Gaussian process model converged given only a limited number of points. Normalized data points were examined for this study and the maximum error was compared after adding one additional data point, Figure 19. The reference value was the value of the model with all the points included and error comparison was taken from 5 points up to 39 points. Taking any fewer than 5 points was physically unreasonable as the parameter space was a 4 dimensional problem. Finding the maximum error in the model across the entire design space proved computationally expensive and a gradient based optimization was used to find the maximum error points. For each run of the model 30 start locations were used for the optimizer to insure that the global maximum was not confused with local maxima.

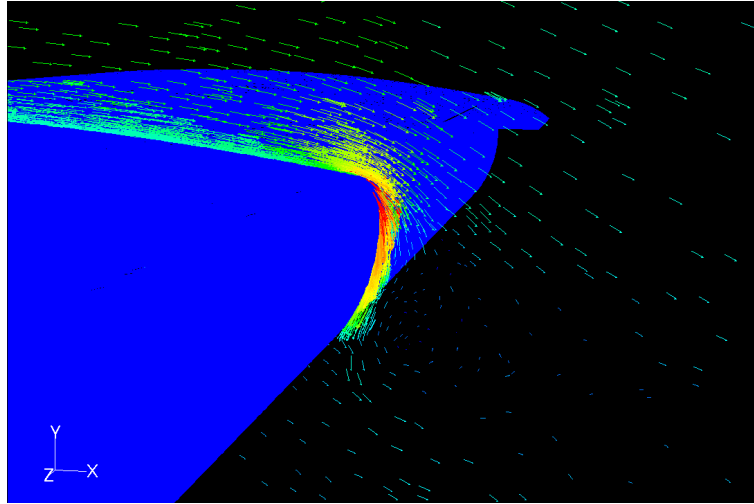


Figure 18: Cut plane of velocity vectors for 3D CCW with recirculation region behind dual radius flap.

The result was that the model seemed to reach a steady state value around 30 points with more points only providing a marginal increase in model accuracy. Ideally these values could be compared to experimental models and validated.

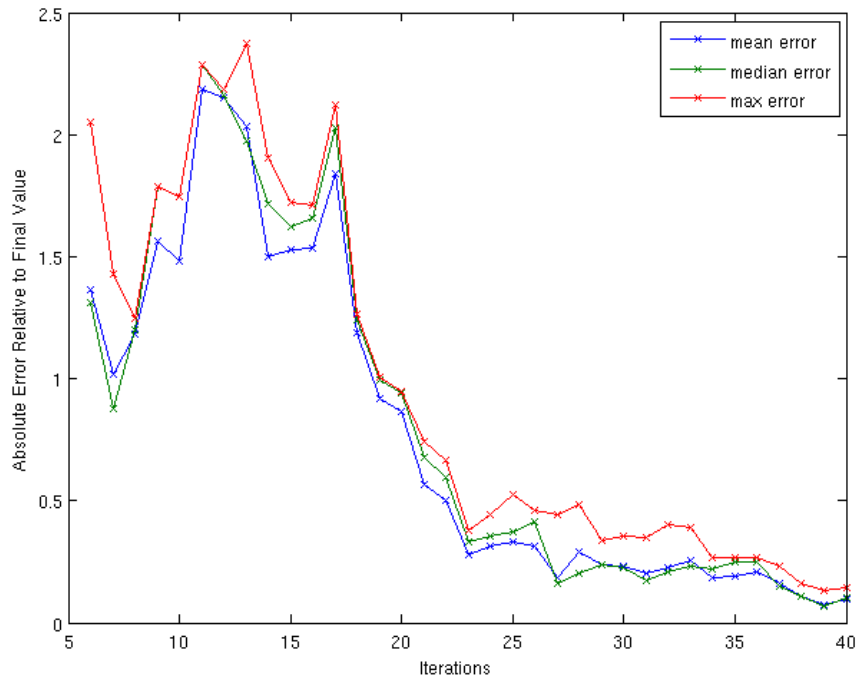


Figure 19: Error Convergence for Gaussian process based on normalized input data

VIII. BFL Model

With a metamodel constructed it was possible to build a balanced field length code that integrated the equations of motion and used the Gaussian process model as the aerodynamic model for the aircraft. The equations of motion were coded in Matlab using the following assumptions to simplify the implementation of the model. Rotation was implemented as three seconds of additional ground roll after which the angle of attack was set to the climb angle of attack. Moments were ignored and rotation was assumed to be possible. Transition was not included and climb was assumed to follow rotation. A simplified block diagram shows one loop of the BFL code and which model is used in which segment of the takeoff calculation. This resulted in a 3 degree of freedom model.

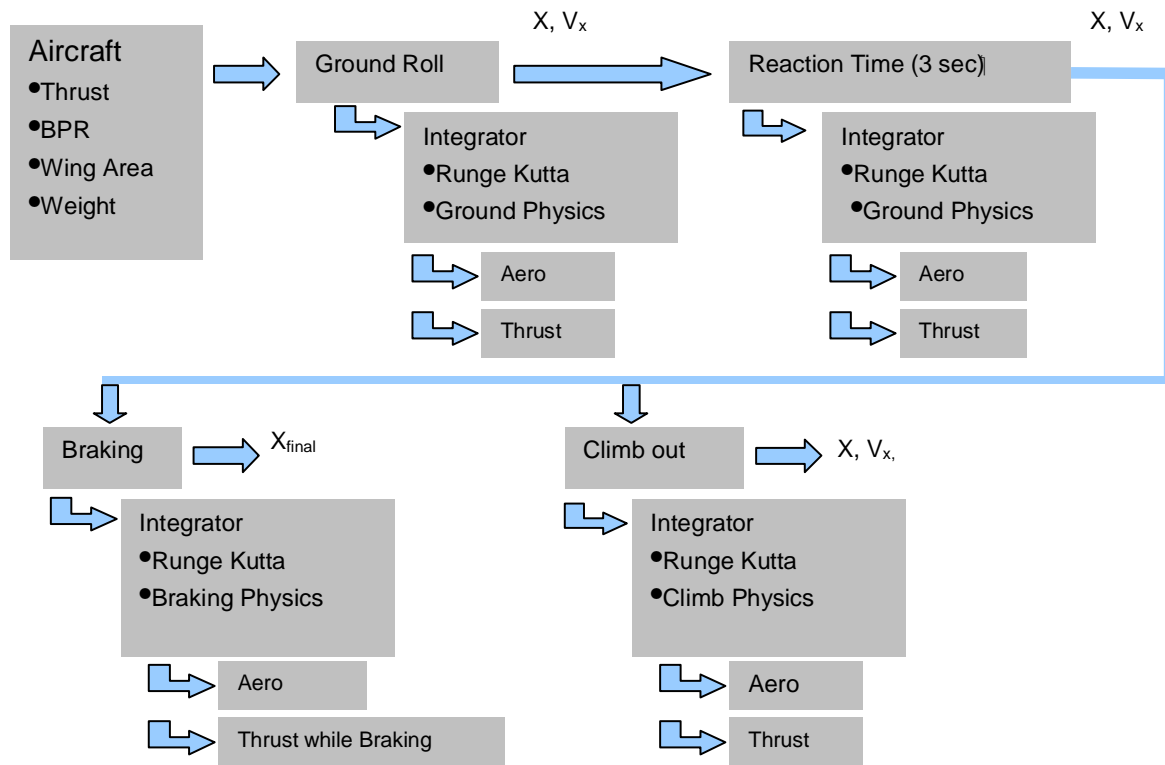


Figure 20: Block Diagram of Takeoff Model

There are additional assumptions that are built into the aerodynamics and thrust models. The thrust model follows a quadratic variation of air speed, which was determined from three known datapoints for two validation models. The aerodynamic model was assumed to be uncoupled from the propulsion model by the use of imbedded gas generators for the mass flow production. The drag of the wing is taken to be the total drag of the aircraft and no ground effect was taken into account.

A Runge Kutta ordinary differential equation solver was used to integrate the equations of motion at different points in the ground roll. Each segment has a separate integrator so that different conditions could be implemented with the same physics model. For instance, while the rotation/reaction interval uses the same physics as the ground roll, it would be possible to switch out that physics model and integrate across a rotation as well as a velocity. The modular format also allows for implementation of different aero and thrust functions at different points in the takeoff. As will be examined in detail, the mass flow rate could be changed mid take off and the effect could be compared with a quadratic increase in mass flow. The architecture structure leaves room for many types of preliminary takeoff analysis all that is required is a thrust model, an aerodynamics model, and some basic aircraft parameters.

IX. Performance Validation

In order to determine whether the results provided by our model were accurate, it was necessary to compare them to known results. Two validation cases were taken from an undergraduate study of preliminary takeoff analysis programs¹⁷. Among other things, the report aimed to compare different methods for using the equations of motion to analyze takeoff and compare those to known results. The known results which were used to validate the current model included data for the McDonnell Douglas DC-9 from NASA Langley's Flight Optimization System (FLOPS) and also flight test data for a Boeing 747-400 from reference 18. Those results were compared to two existing methods. Those methods were "the simplified method proposed by Powers¹⁹ and the modified version of the method proposed by Krenkel and Salzman²⁰."

Since the DC-9 FLOPS results included the results for BFL, it became the first validation case for the model. All of the aircraft parameters that were input into the FLOPS model were also included with reference 12 and were easily entered into the current model. These parameters included the quadratic thrust model, thrust, weight, wing area, and the assumed C_L and C_D for the different phases of takeoff. The detailed CC aerodynamic block was replaced with the simplified assumptions which were used in the FLOPS model in order to match the results. The only significant different between the two models was the method for determining the rotation velocity. This validation case employed the modified rotation velocity calculation previously described which varies from

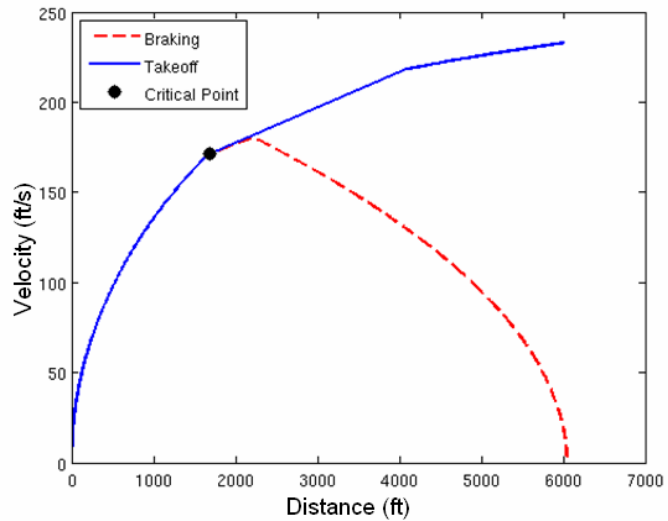


Figure 21: DC-9 Validation BFL

Table 2: DC-9 Validation Results

Parameter	Our Model	FLOPS	% Difference
V_r (ft/s)	198.2	221.3	10.56
V_{lo} (ft/s)	218.18	249.1	12.41
V_{ob} (ft/s)	247.77	268.3	7.65
S_{to} (ft)	4218	4397	4.07
BFL (ft)	6027	5623	7.18

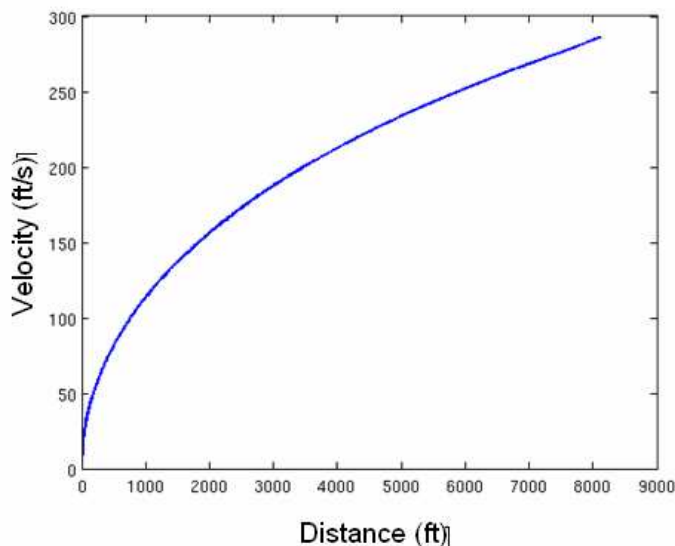


Figure 22: Takeoff Validation for 747

traditional methods. FLOPS was assumed to use these traditional methods. With all of the input data entered into the current model, the BFL was calculated and the results are illustrated in Figure 21 and listed in Table 2. Although the different velocities tended to vary up to 12% from the FLOPS results, the overall distances were much closer with takeoff and BFL being about 4 and 7% different respectively. It is also interesting to note that the rotation velocities were relatively close with the modified rotation method predicting the occurrence at about 10% slower speeds. This variance seems reasonable when considering the assumptions that were made deriving the modified method.

The other validation case was that of a 747-400 with its flight test results¹⁷⁻¹⁸. Since the known results were from a flight test, it was difficult to reconstruct an actual airplane to fit into a preliminary takeoff model. The same assumptions about thrust, lift, and drag which were used by reference 17 in the Powers and modified Krenkel and Salzman codes since they performed well at matching the test results within about 5%. However, there did exist a discrepancy for the lift off distance with the Powers method producing a distance over 20% shorter than the given 7,500 ft¹⁷. At any rate, the input parameters were entered into the current model. At first, there

Table 3: 747 Validation Results

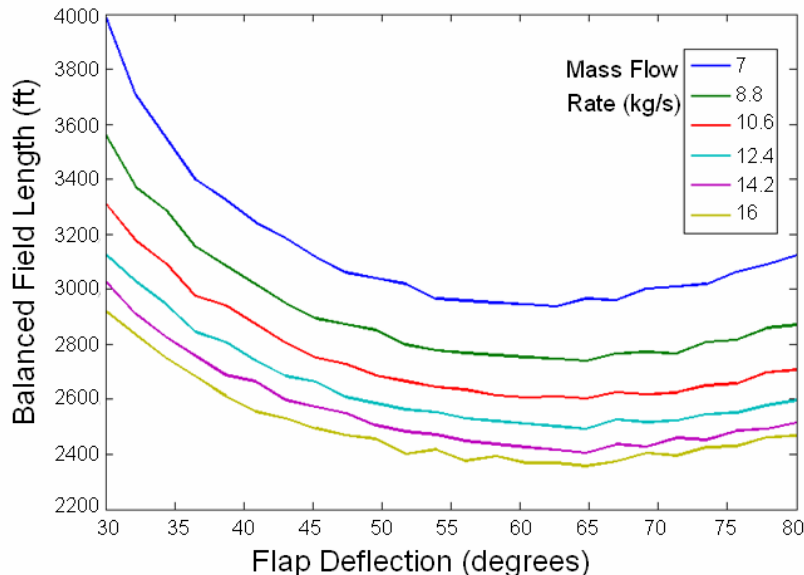
Parameter	Our Model	Flight Test	% Difference
V_r (ft/s)	264	271	2.58
V_{lo} (ft/s)	275.78	283.4	2.79
V_{ob} (ft/s)	285.2	288.8	1.25
S_{to} (ft)	8123	8645	6.04

very well with the flight test with error of the overall takeoff distance decreasing from 18 % to 6% and the other velocities all matching within 3% or better. Although the traditional rotation calculations agreed better with the test data in this case, more research will have to be put forth to improve the idea that the rotation speed can be a function of lift over weight rather than solely C_{Lmax} . Robert Englar²¹ has also addressed this problem and future results may encompass some of his work to better improve the rotation model. It is also worth noting that some of the error could have originated from the input data for the 747 since the Powers results¹⁷ also differed greatly from the test data. More test data or FLOPS results are needed to fully validate the model and the modified rotation velocity calculations. However, the model itself has shown that it works well at predicting takeoff performance for some traditional aircraft and next the results of a CC STOL transport will be analyzed.

was a significant (about 18%) difference between the takeoff distances. It was thought that it was possibly the modified rotation calculation causing some of the error so the case was run again with the traditional method for calculating rotation velocity based on the given C_{Lmax} . Those results can be seen in Figure 22 and tabulated in Table 3. With the traditional rotation velocity calculation, the results matched

X. Performance of STOL Aircraft

With the BFL code verified, a flap deflection and mass flow rate study was completed to determine optimal settings for BFL reduction. The result was that balanced fields lengths as low as 2400 feet could be achieved but those were obtained with diminishing returns since mass flows of 20% less could obtain a BFL of 2500 feet. This analysis was based on a STOL transport designed for the 2007 AIAA undergraduate design competition. This gave a design for which numbers for drag, engine sizing, and airfoil performance were well known to the authors. Perhaps most importantly, it gave a thrust, weight and wing area that were designed for a 2500 foot BFL, which helped with debugging and is also the

**Figure 23: STOL Transport Concept****Figure 24: Variation in BFL for STOL concept with varying Mass Flow and Flap Deflection****Table 4: Transport Parameters**

Thrust (lbs)	130,000
Wing Area (ft ²)	2,200
Weight (lbs)	230,000
T/W	0.565

range of current industry STOL transport work. Some basic stats for the aircraft are shown in Table 4. The thrust was increased above the original design up to 130,000 lbf, to provide a wider range of feasible takeoff conditions. The results of the mass flow and flap deflection study are shown in Figure 24.

As the flap deflection is increased there becomes a point where a minimum BFL is reached for any particular mass flow rate. This is due to the loss of supercirculation caused by separation, not over the entire

wing, but just aft of the flap. One might expect that there would be a sharp change at this point due to increased drag caused by the recirculation, but after looking at the metamodel and data points, it was noticed that the drag actually goes down in the regions that experience separated flow off of the flap. The reason the total drag decreases is the loss of lift and reduction of induced drag. This decrease in drag helps BFL while the loss in lift acts in the opposite direction. The net overall effect is that the shape of the curve changes radius of curvature as compared to the small flap deflections and the BFL distances go up at a slower rate than they decreased.

The mass flow rate term, unlike the flap, always provides an additional benefit to BFL, but the amount by which it improves is clearly diminishing. As mentioned above, for a 22% decrease in mass flow, you lose only 4% of your balanced field length (2400 feet to 2500 feet). A possible explanation of this is that with additional flow the shear layer has a higher gradient across it and little additional energy is transferred into the adjoining flow. And finally, it is interesting to note that for high mass flow rates, the effect of flap deflection decreases.

The second major performance analysis was performed to determine the effects of varying the mass flow rate and flap deflection at different points in the takeoff. Specifically, it was the goal to determine the benefits of delaying the mass flow or flap deflection in order to reduce induced drag and therefore aid in the acceleration in the ground roll. Both flap deflections and mass flow were varied separately throughout the ground roll and compared to cases where they were held constant.

The first case which was explored was the delay in mass flow rate. The flap was held constant throughout these cases at the previously found optimum of 64° . Two different mass flow variations were investigated: 1) a switch from essentially no mass flow to either 10 or 20 kg/s at a designated velocity in the ground roll and 2) vary the mass flow quadratically from zero to either 10 or 20 kg/s. The first case will be designated as the “step” input of mass flow while the second as the quadratic variation. Four cases of step inputs were examined which involved stepping at 100 or 180 ft/s and for each of those, stepping to 10 or 20 kg/s. Two cases of quadratic variations were examined involving increasing the mass flow from zero to a maximum of 10 or 20 kg/s at 180 ft/s. An illustration of the step and quadratic variations to 20 kg/s is shown in Figure 25. The step input of mass flow at 100 ft/s is clearly visible with the drastic decrease in L/D at that point. By examining Figure 26 it can be seen that although the C_L at that point jumped roughly from 1.5 to 3.5, the C_D jumped from 0.2 to 0.8 which in turn decreased the L/D value. This clearly shows one of the major difficulties of a powered lift aircraft which is that producing a lot of lift also produces a lot of induced drag. This is the reason why most STOL transports have thrust to weight ratios near or above 0.5. The quadratic variation is

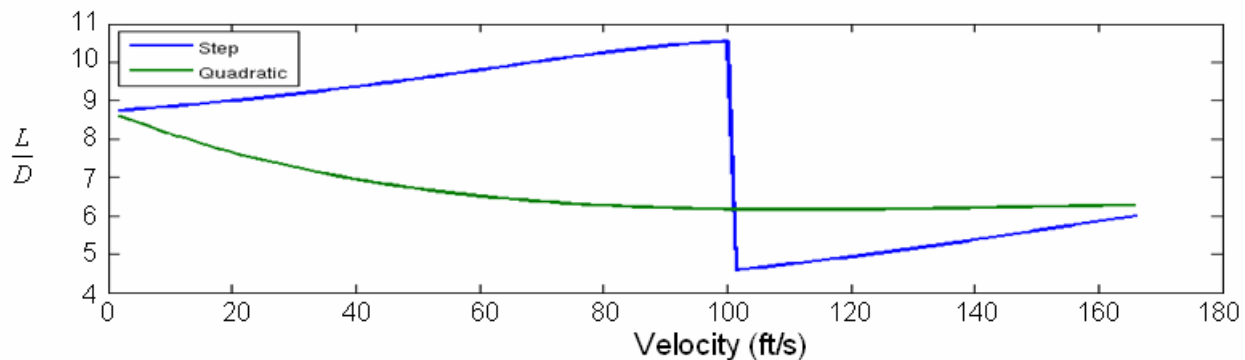


Figure 25: L/D of a Takeoff with Variations in Mass Flow Rate

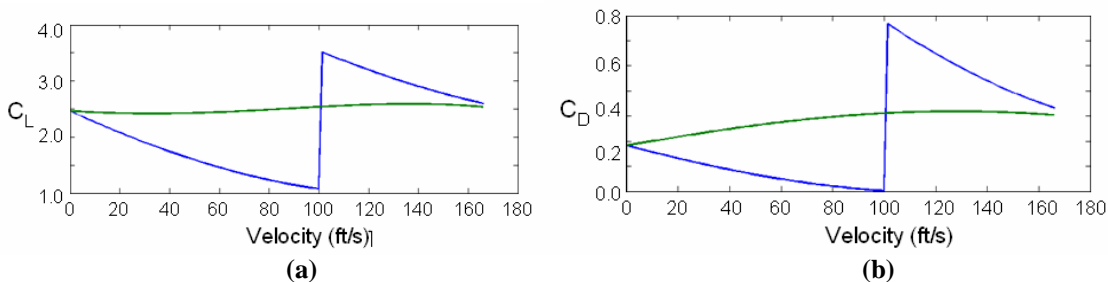


Figure 26: Variations in a) C_L and b) C_D over Takeoff with Varying Mass Flow Rate

also of interest to examine. The C_L actually remained almost constant at a value of about 2.5 throughout the entire takeoff. The reason it remained constant was due to the effect of Mach number on CC which had been discovered previously with the metamodel. As the Mach number increased, the ability of the mass flow to entrain the freestream flow decreased and therefore the lift decreased. This decrease in performance for the CC was counteracted by the quadratic increase of mass flow. This may prove to be a useful comparison to traditional flapped wing takeoff since they generally are engaged for the entire ground roll providing a constant C_L . The results from all of the different mass flow trials can be seen in Table 5. From examining the results, it is clear that the largest decrease in BFL and takeoff distance occurred with the step variation of mass flow at the later speed. The maximum change occurred in the BFL distance with the 20 kg/s mass flow step at 180 ft/s which decreased 8.66% from the BFL with the mass flow

Table 5: Results for Mass Flow Variations

		Speed at which Blowing was Turned on (ft/s)						
		100		180		Quadratic Increase to 180		Whole Time
		actual	% decrease	actual	% decrease	actual	% decrease	actual
10 kg/s Mass Flow	Takeoff Distance (ft)	2512	0.95	2479	2.25	2515	0.83	2536
	BFL (ft)	2776	1.14	2692	4.13	2775	1.18	2808
20 kg/s Mass Flow	Takeoff Distance (ft)	2191	0.63	2068	6.21	2157	2.18	2205
	BFL (ft)	2395	1.68	2225	8.66	2357	3.24	2436

blowing the entire time. The only issue which would need to be resolved in order to perform such a takeoff would be the reliability of the mass flow source. Also, it is important to note that all of the results used in this model occur at steady state and take no account of any transient behavior of turning on or diverting the mass flow source.

The next performance analysis involved keeping the mass flow steady and varying the deflection of the dual radius flap throughout the takeoff. A similar set of cases were set up as for the mass flow variations with the flap having a step variation at certain speeds and also varying the flap quadratically as before. These tests were performed with the same two mass flow rates, 10 and 20 kg/s, and the step and quadratic variations behaved in a similar way as before only with the flap deflection instead of the mass flow. The results for a couple of the 20 kg/s trials are shown in Figure 27. The results are surprisingly similar to the variations in mass flow with only a few exceptions. For both the step and quadratic variations shown, the ratio of lift to drag begins much lower than before and the step function increases at a faster rate while the quadratic variation remains almost perfectly steady at its initial value. The behavior

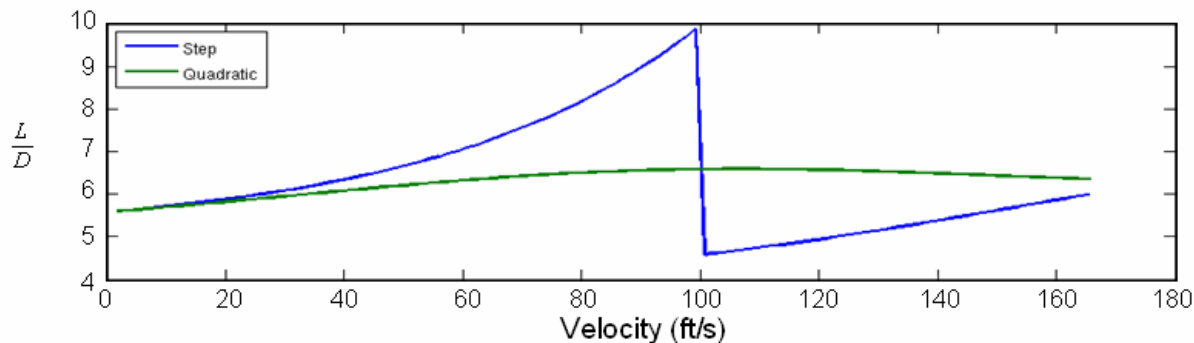


Figure 27: L/D throughout Takeoff with Flap Variations

of lift and drag individually can also be seen in Figure 28. The only major change between these results and those with the varying mass flow is a large increase in the C_D at the start of the takeoff run which is the source of the difference between the two L/D curves. It appears that there is a significant increase in drag with an addition of mass flow regardless of the flap deflection. The final numbers for the varying flap cases can be seen in Table 6. The actual decreases in BFL and takeoff were remarkably similar to those seen with the variable mass flow. The best performance again was found with the latest flap deflection with the highest mass flow with roughly a 9% decrease in BFL. There is a potential benefit in complexity and reliability if only a small 10% chord flap need be deflected rather than a large amount of mass flow diverted. In either case, it is interesting to note that for the same aircraft, the balanced field length could be shortened by up to 8% simply by delaying either the dual radius flap deflection or the mass flow out of the ejection slot.

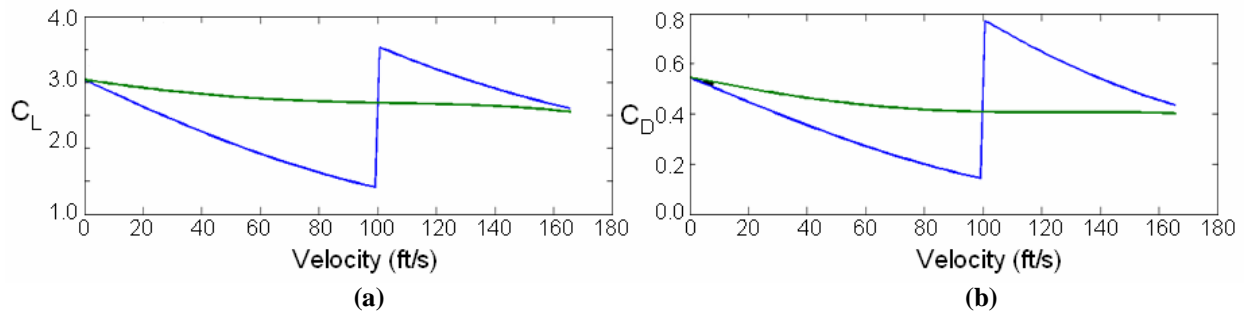


Figure 28: Variations in a) C_L and b) C_D during Takeoff with Flap Variations

Table 6: Results for Variable Flap Deflections

		Speed at which Flap was Deflected to 64°						
		100		180		Quadratic Increase to 180		Whole Time
		actual	% decrease	actual	% decrease	actual	% decrease	actual
10 kg/s Mass Flow	Takeoff Distance (ft)	2514	0.87	2441	3.75	2533	0.12	2536
	BFL (ft)	2780	1	2656	5.41	2780	1	2808
20 kg/s Mass Flow	Takeoff Distance (ft)	2185	0.91	2069	6.17	2190	0.68	2205
	BFL (ft)	2385	2.09	2217	8.99	2387	2.01	2436

XI. Acknowledgements

This work was sponsored by the Department of the Navy, Office of Naval Research, under Award # N00014-06-1-1111.

XII. Conclusion

The objective of this research study was to produce a model which could accurately predict the takeoff and balanced field length performance of a powered lift aircraft, specifically with circulation control. The current techniques for preliminary takeoff performance analysis were analyzed and were determined to be inadequate for powered lift aircraft. This inadequacy stemmed from the traditional methods being developed for traditional aircraft and therefore having no account for powered lift such as circulation control or variations in thrust, lift, or drag with Mach number. Additionally, a new concept for determining the rotation velocity was also developed which relied solely on a lift to weight ratio rather than being a function of C_{Lmax} because of the difficulty of defining C_{Lmax} with circulation control. In order to develop a better aerodynamic model to account for the effects of circulation control during takeoff, a 4-D design space consisting of Mach number, angle of attack, mass flow rate, and flap deflection was created and discretized in the manner of a Monte Carlo. CFD was performed at 40 different random points in that design space for the given circulation control wing. Those results were fed into a metamodel which utilized Gaussian Processes in order to create an aerodynamic function which could be used to interpolate and extrapolate the CFD data as needed. That aerodynamic function was then inserted into takeoff/BFL code in order model circulation control takeoff performance. The model examined the performance of a STOL transport with parameters varied such as flap deflection and mass flow rate in order to obtain optimal balanced field lengths. For the transport which was examined, it was found that a 64° flap achieved the shortest BFLs and that mass flow rates higher than 12 kg/s had diminishing returns. For the same STOL transport, the takeoffs were altered so that the mass flow rate or the flap deflection varied in order to determine whether or not the reduced induced drag had a significant effect on BFL. It was found that both delaying the mass flow and flap deflection resulted in almost identical decreases in takeoff and BFL. The highest decrease about 8% in BFL for both cases occurred with the flap deflection or mass flow delayed until the ground speed reached 180 ft/s.

References

- ¹Mayfield, Jerry. "Circulation Control Demonstrates Greater Lift." *Aviation Week and Space Technology*, March 19, 1979.
- ²Anderson, John D. *Aircraft Performance and Design*. McGraw-Hill Science Engineering, New York. Ch 6. 1998.
- ³Federal Aviation Administration. Regulatory and Guidance Library.. Washington D.C. 2007. Part 25: 105, 107, 109, 111, 113, 121. http://rgl.faa.gov/Regulatory_and_Guidance_Library
- ⁴Torenbeek, Egbert. *Synthesis of Subsonic Airplane Design*. Delft University Press, Delft, The Netherlands. Ch5 and App. K 1982.
- ⁵Englar, Robert J. Overview of Circulation Control Pneumatic Aerodynamics: Blown Force and Moment Augmentation and Modification as Applied Primarily to Fixed-Wing Aircraft. NASA/ONR Circulation Control Workshop, March 16-17, 2004, NASA/CP-2005-213509.
- ⁶Englar, Robert J., and Gregory G. Huson. "Development of Advanced Circulation Control Wing High-Lift Airfoils." *Journal of Aircraft*, Vol. 21, No. 7, (1984): 476-483.
- ⁷Hall, Dave et. al. Summer 2004 CalPoly/NASA ESTOL Work Presented to NASA/Ames ESTOL Vehicle Systems Sector. PowerPoint Presentation. August 27, 2004.
- ⁸Abramson, J., and E.O. Rogers. *High-Speed Characteristics of Circulation Control Airfoils*. AIAA-83-0265.
- ⁹Percey, Bobbitt J., Eagle Aeronautics, Margason, Richard. *Analysis of the Take-off and Landing of Powered Lift Aircraft*. American Institute of Aeronautics and Astronautics, Inc., 2007
- ¹⁰Jones, Gregory S., and Ronald D. Joslin. *Introduction: 2004 NASA/ONR Circulation Control Workshop*. 2004 NASA/ONR Circulation Control Workshop, March 16-17, 2004, NASA/CP-2005-213509
- ¹¹Liu, Yi, Sankar, Lakshmi N., Englar, Robert J., Ahuja, Krishan K. *Numerical Solutions of the Steady and Unsteady Aerodynamic Characteristics of a Circulation Control Wing*. GTRI Report A5928/2003-1 App. B. Georgia Tech Research Institute, GA 2003.
- ¹²Koehler, J.R., Owen, A.B. "Computer Experiments," *Handbook of Statistics*, Elsevier Science, vol.13, pp.261-308, 1996
- ¹³Box, George E.P., Draper, Norman R. *Reponse Surfaces, Mixtures, and Ridge Analysis*. John Wiley & Sons, Inc., Hoboken New Jersey, 2007
- ¹⁴Rasmussen, Carl Edward, Williams, Christopher K.I. *Gaussian Processes for Machine Learning*. The MIT Press, Cambridge Massachusetts, 2006
- ¹⁵McDonald, Robert A. *Error Propagation and Metamodeling for a Fidelity Tradeoff Capability in Complex System Design*. Ph.D Thesis, Georgia Institute of Technology, GA, 2006
- ¹⁶Englar, Robert J. "Overview of Circulation Control Pneumatic Aerodynamics: Blown Force and Moment Augmentation and Modification as Applied Primarily to Fixed-Wing Aircraft," *Progress in Astronautics and Aeronautics*, vol.214, American Institute of Aeronautics and Astronautics, pp. 23-64, 2006.
- ¹⁷Lynn, Sean. *Summary Report for an Undergraduate Research Project to Develop Programs for Aircraft Takeoff Analysis in the Preliminary Design Phase*, Undergraduate Research Project, Virginia Polytechnic Institute and State University. Blacksburg, VA. May 11, 1994.
- ¹⁸Hank, C.R., et al, "The Simulation of a Jumbo Jet Transport Aircraft. Volume 2: Modeling Data," NASA CR 114494, also N73-10027 Sept. 1970.
- ¹⁹Powers, S. A., "Critical Field Length Calculations for Preliminary Design," *Journal of Aircraft*, Vol. 18, No. 2, 1981
- ²⁰Krenkel, A.R., Salzman, A., "Takeoff Performance of Jet-Propelled Conventional and Vectored-Thrust STOL Aircraft," *Journal of Aircraft*, Vol. 5, No. 5, 1968
- ²¹Englar, Roert J, Smith, Maryillyn J., Kelley, Sean M., Rover, Richard C, III. *Development of Circulation Control Technology for Application to Advanced Subsonic Transport Aircraft*. Aerospace Laboratory, Georgia Tech Research Institute, Atlanta, GA. AIAA 1993-0644